Supplementary Information for

Structural basis for electromechanical coupling and pore block of human $Ca_V1.4$

Yitong Sun[1,4], Tong Wu[1,4], Tongtong Wang[1], Huan Wang[1], Jian Huang[2],

Nieng Yan[1,2,3,5] and Zhangqiang Li[1,5]

[1]State Key Laboratory of Membrane Biology, Beijing Advanced Innovation Center for Structural Biology, Tsinghua-Peking Joint Center for Life Sciences, School of Life Sciences, Tsinghua University, Beijing 100084, China

[2]Institute of Bio-Architecture and Bio-Interactions (IBABI), Shenzhen Medical Academy of Research and Translation, Guangming District, Shenzhen 518107, Guangdong Province, China

[3]Institute of Chemical Biology (ICB), Shenzhen Bay Laboratory, Guangming District, Shenzhen 518132, Guangdong Province, China

[4]These authors contributed equally to this work

[5]To whom correspondence should be addressed: N. Yan (nyan@tsinghua.edu.cn) or Z. Li (lizhangq@tsinghua.edu.cn).

This PDF file includes:

Figures S1-10

Tables S1-2

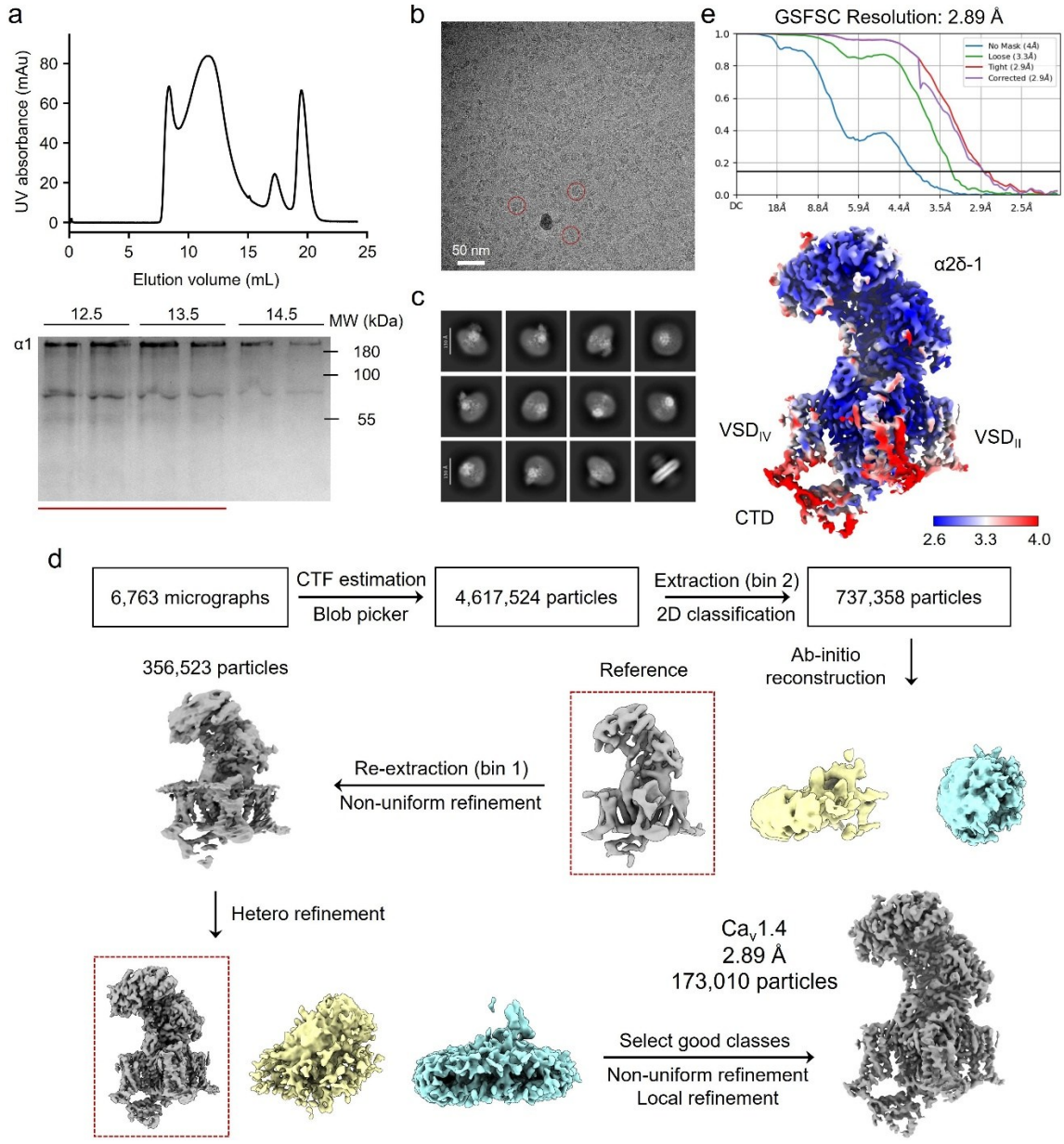

Figure S1 | Cryo-EM data analysis of the human Ca$_v$1.4 complex.

a, Size-exclusion chromatography and Coomassie blue staining analysis of the human Ca$_v$1.4 complex after two-step affinity purification. The indicated fractions were collected and concentrated for cryo-sample preparation. **b,** Representative cryo-EM micrograph of Ca$_v$1.4 complex. Particles with distinct views are indicated by red circles. Scale bar: 50 nm. **c,** Representative 2D class averages of Ca$_v$1.4 complex. Scale bar:

150 Å. **d,** Flowchart of cryo-EM data processing for $Ca_v1.4$ complex. Details can be found in Methods. **e,** Local resolution distribution and Golden Standard Fourier Shell Correlation (GSFSC) curve for the 3D reconstruction of $Ca_v1.4$ complex. All EM maps were contoured at 6 σ unless otherwise specified.

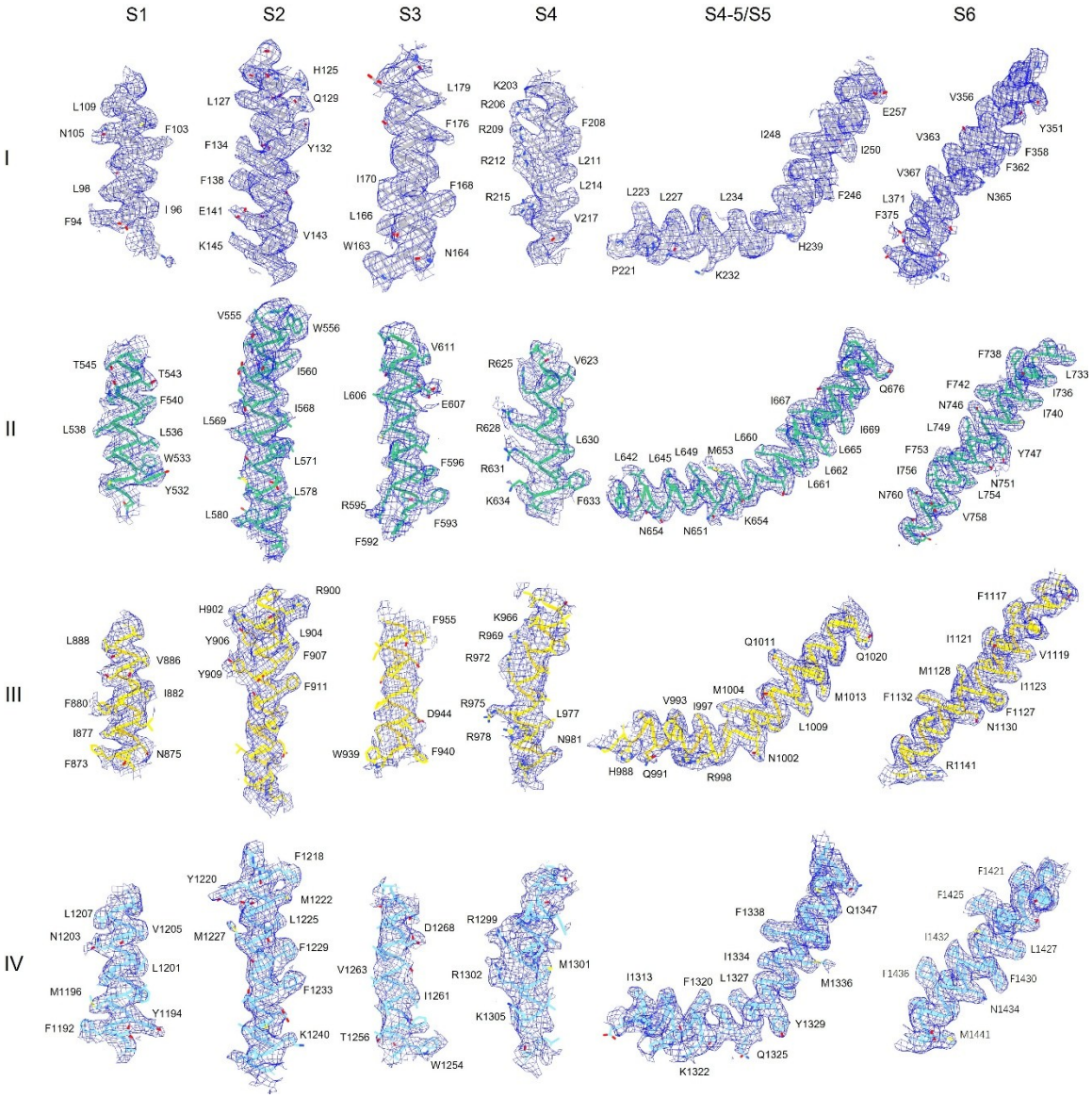

Figure S2 | EM maps for representative segments of $Ca_v1.4$.

EM maps for the transmembrane segments in each repeat of $Ca_v1.4$ α1 subunit. The densities are shown at a contour level of 4.5 σ.

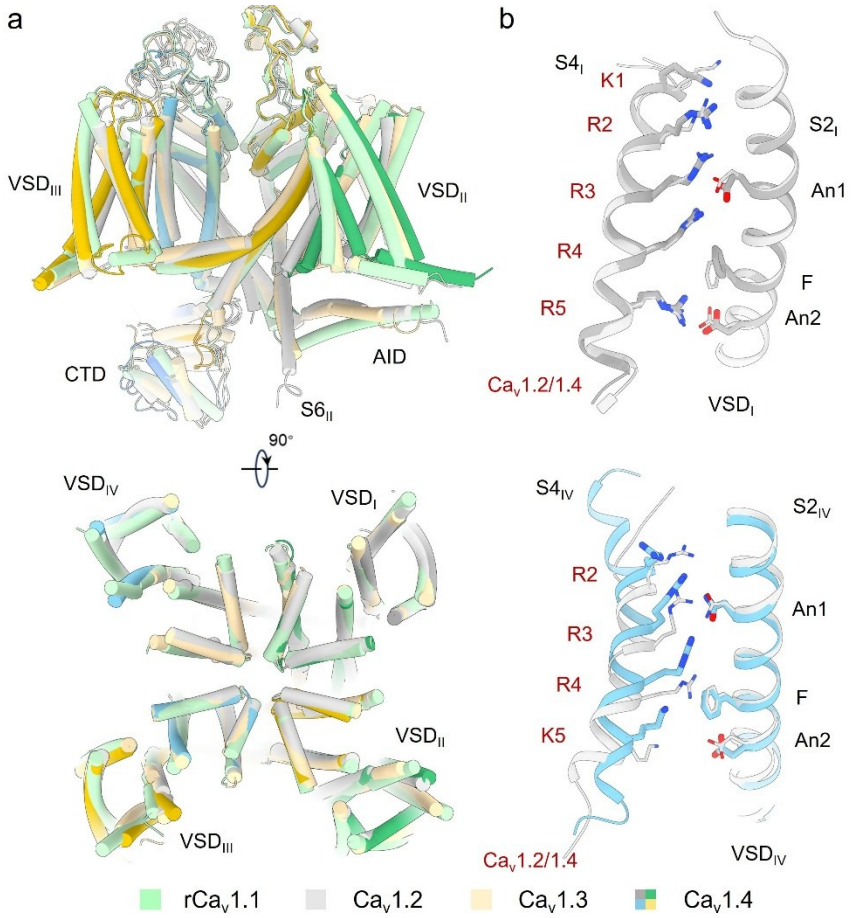

Figure S3 | Structural comparison of Ca$_v$1.4 with other reported Ca$_v$1 channels.

a, Two perpendicular views of superimposed structures are shown for rCa$_v$1.1 (light green, PDB: 5GJV), Ca$_v$1.2 (light grey, PDB: 8WE6), Ca$_v$1.3 (wheat, PDB: 7UHG), and Ca$_v$1.4 (domain-colored). The extracellular loops (ECLs) are omitted in the left panel for visual clarity. Major structural differences among these channels are observed in VSD$_{II}$.

b, The VSD$_I$ and VSD$_{IV}$ of Ca$_v$1.4 exhibit similar conformations to those of Ca$_v$1.2. Structural superimposition of VSD$_I$ and VSD$_{IV}$ from Ca$_v$1.4 and Ca$_v$1.2 is shown. The S1 helices are omitted for visual clarity.

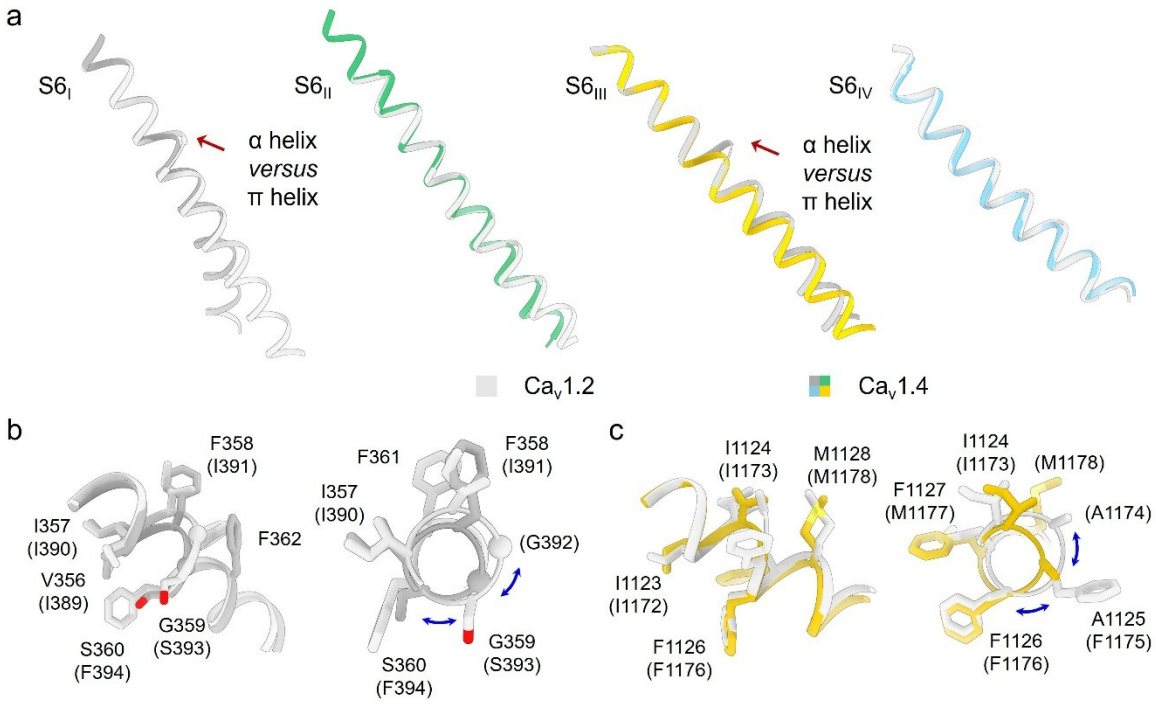

Figure S4 | Distinct structural conformers of S6$_I$ and S6$_{III}$ helices in Ca$_v$1.4.

a, Structural differences of S6 helices between Ca$_v$1.4 and Ca$_v$1.2. Superimposition of S6 helices reveals backbone differences between the α and π conformers. Both S6$_I$ and S6$_{III}$ of Ca$_v$1.4 adopt an α-helical conformation. **b, c,** Differences among α conformers in Ca$_v$1.4 arise from axial rotation of S6$_I$ after G359 (**b**), and of S6$_{III}$ after A1125 (**c**). The residues shown in brackets are from Ca$_v$1.2. Two views are shown.

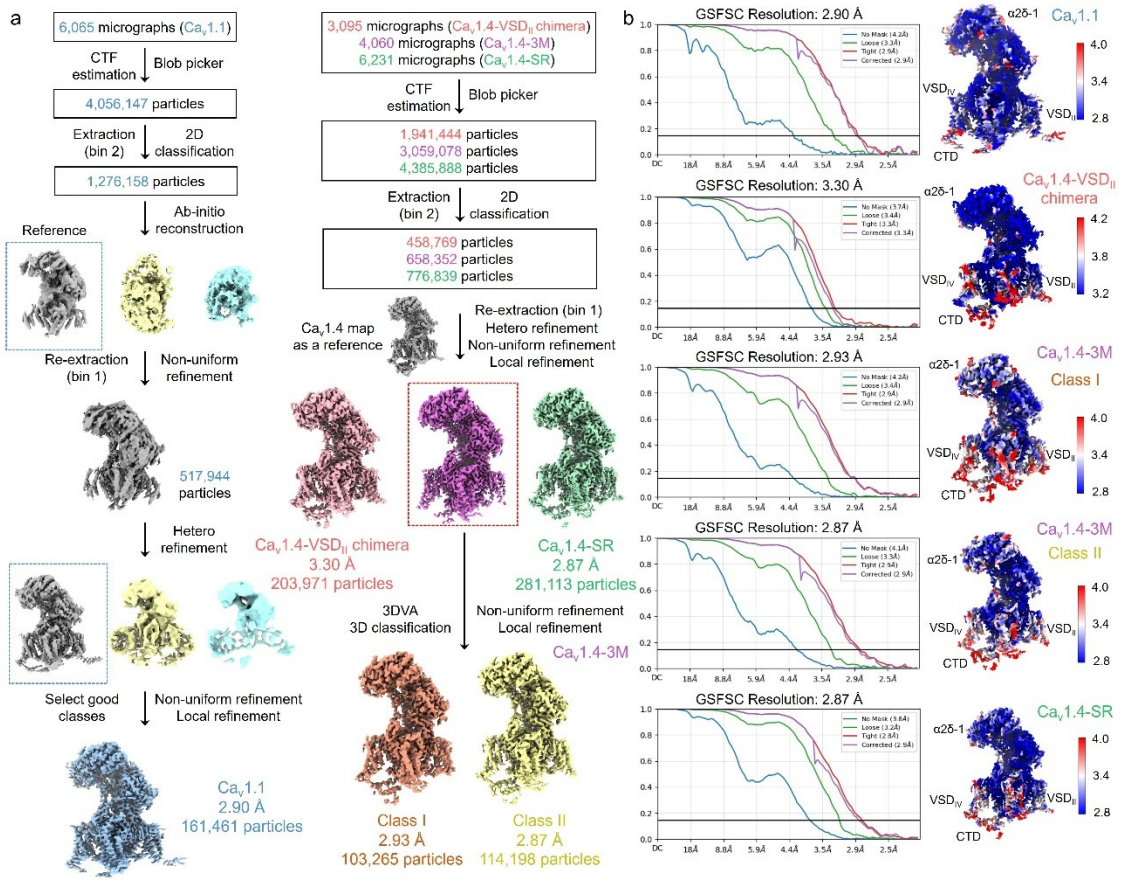

Figure S5 | Cryo-EM data analysis of the human $Ca_V1.1$ complex, $Ca_V1.4$ engineered variants, and $Ca_V1.4$ in complex with SR33805.

a, Flowcharts of cryo-EM data processing for human $Ca_V1.1$ complex, $Ca_V1.4$-$VSD_{II}1.1$ chimera, $Ca_V1.4$-3M, and $Ca_V1.4$-SR33805, respectively. Details can be found in Methods. **b,** Golden Standard Fourier Shell Correlation (GSFSC) curves and local resolution distributions for the 3D reconstructions of human $Ca_V1.1$ complex, $Ca_V1.4$-$VSD_{II}1.1$ chimera, $Ca_V1.4$-3M, and $Ca_V1.4$-SR33805, respectively.

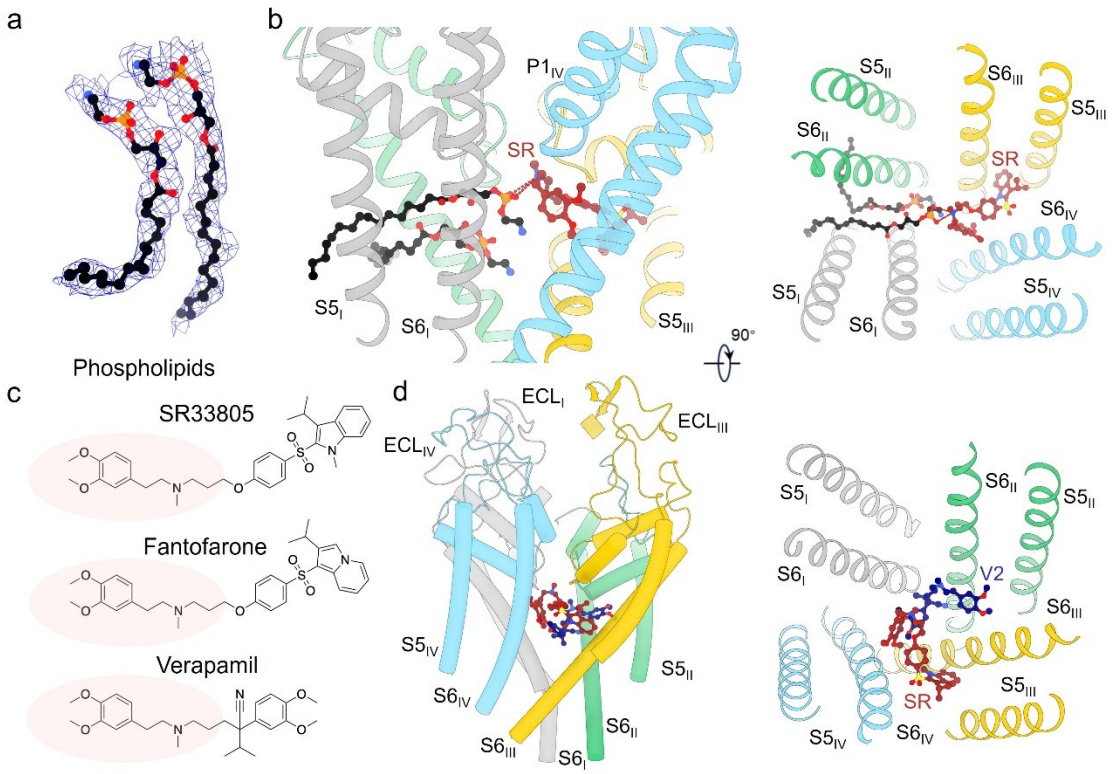

Figure S6 | Cryo-EM analysis of $Ca_v1.4$-SR33805.

a, Local EM density of the endogenous lipid. The EM map is contoured at 4 σ. **b,** The endogenous lipid stabilizes SR33805 binding in the central cavity of $Ca_v1.4$. Red dashed line indicates the potential H bond. **c,** Chemical structures of SR33805, fantofarone, and verapamil. The common chemical groups in these molecules are highlighted by the transparent pink oval. **d,** Structural comparison of SR33805 and verapamil (V2). Shown here are two perpendicular views. For clarity, only the PD of $Ca_v1.4$ is displayed. SR33805 and verapamil (V2) exhibit distinct binding poses, where SR33805 penetrates the fenestration formed by repeats III and IV, whereas verapamil (V2) is located near repeats II and III.

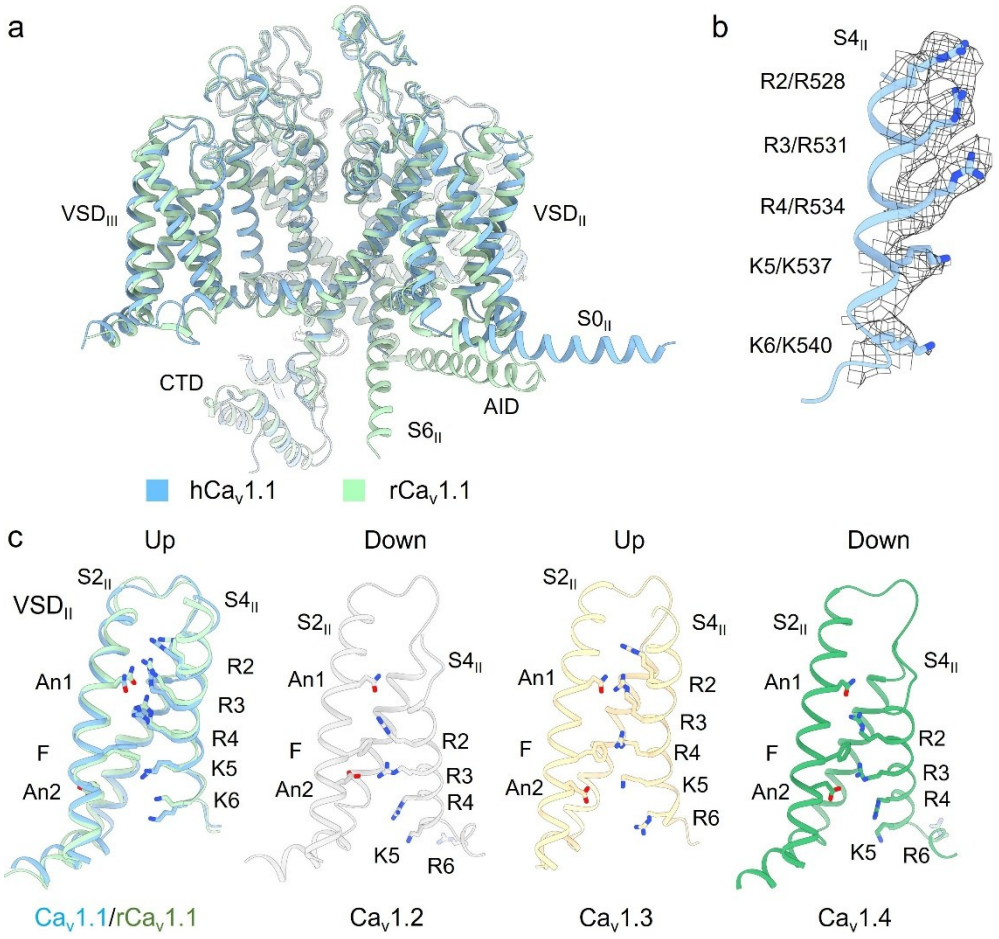

Figure S7 | Structural variations of VSD$_{II}$ in Ca$_v$1 channels.

a, Structural comparison of human Ca$_v$1.1 and rabbit Ca$_v$1.1 reveals nearly identical conformations. **b,** Local EM density for S4$_{II}$ of human Ca$_v$1.1. The EM density is contoured at 6 σ. **c,** Structural analysis indicates that the VSD$_{II}$ of human Ca$_v$1.1, rabbit Ca$_v$1.1, and Ca$_v$1.3 exhibits an "up" conformation, whereas that of Ca$_v$1.2 and Ca$_v$1.4 adopts a "down" conformation. Human Ca$_v$1.1 is colored light blue, while the other Ca$_v$1 channels are colored according to the scheme used in Figure S3.

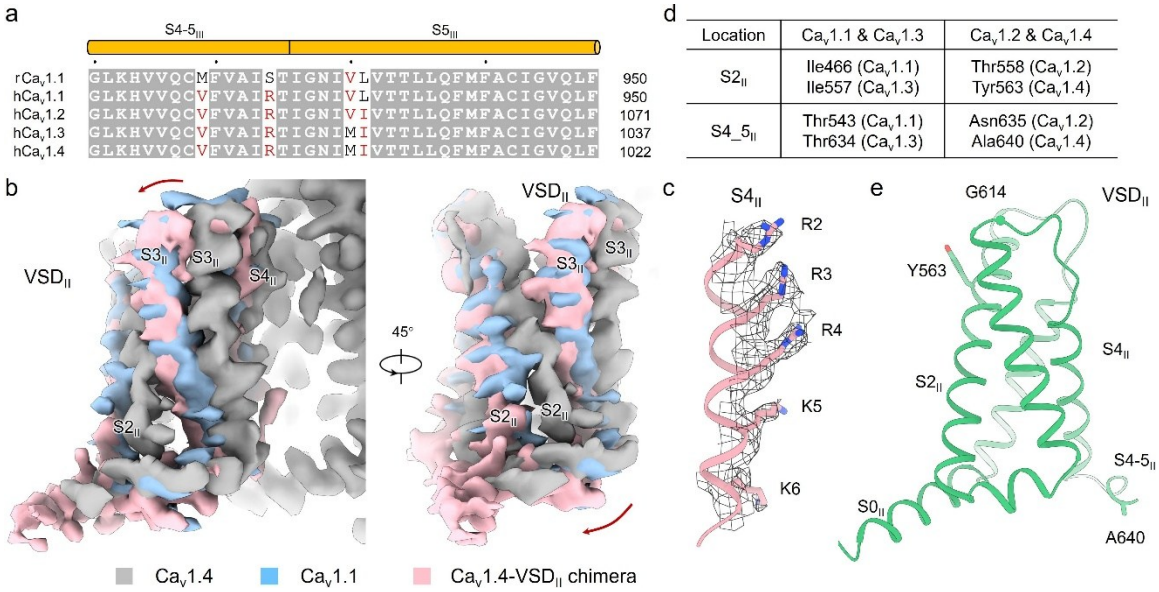

Figure S8 | Structural analysis of VSD_{II} in different conformations across Ca_v1 channels.

a, Sequence alignment of $S4\text{-}5_{III}$ among Ca_v1 channels. **b,** Compared with $Ca_v1.4$, the VSD_{II} of $Ca_v1.4$-$VSD_{II}1.1$ chimera adopts a conformation resembling that of human $Ca_v1.1$. The EM maps for $Ca_v1.4$, human $Ca_v1.1$, and $Ca_v1.4$-$VSD_{II}1.1$ chimera are shown in grey, light blue, and pink, respectively. **c,** Local EM density for $S4_{II}$ of $Ca_v1.4$-$VSD_{II}1.1$ chimera. The EM density is contoured at 6 σ. **d,** Sequence analysis identifies two residues that are conserved in $Ca_v1.1$ and $Ca_v1.3$, but variable in $Ca_v1.2$ and $Ca_v1.4$. **e,** Locations of the three mutated residues. Y563 is located on $S2_{II}$, G614 in S3-4 loop, and A640 in $S4\text{-}5_{II}$.

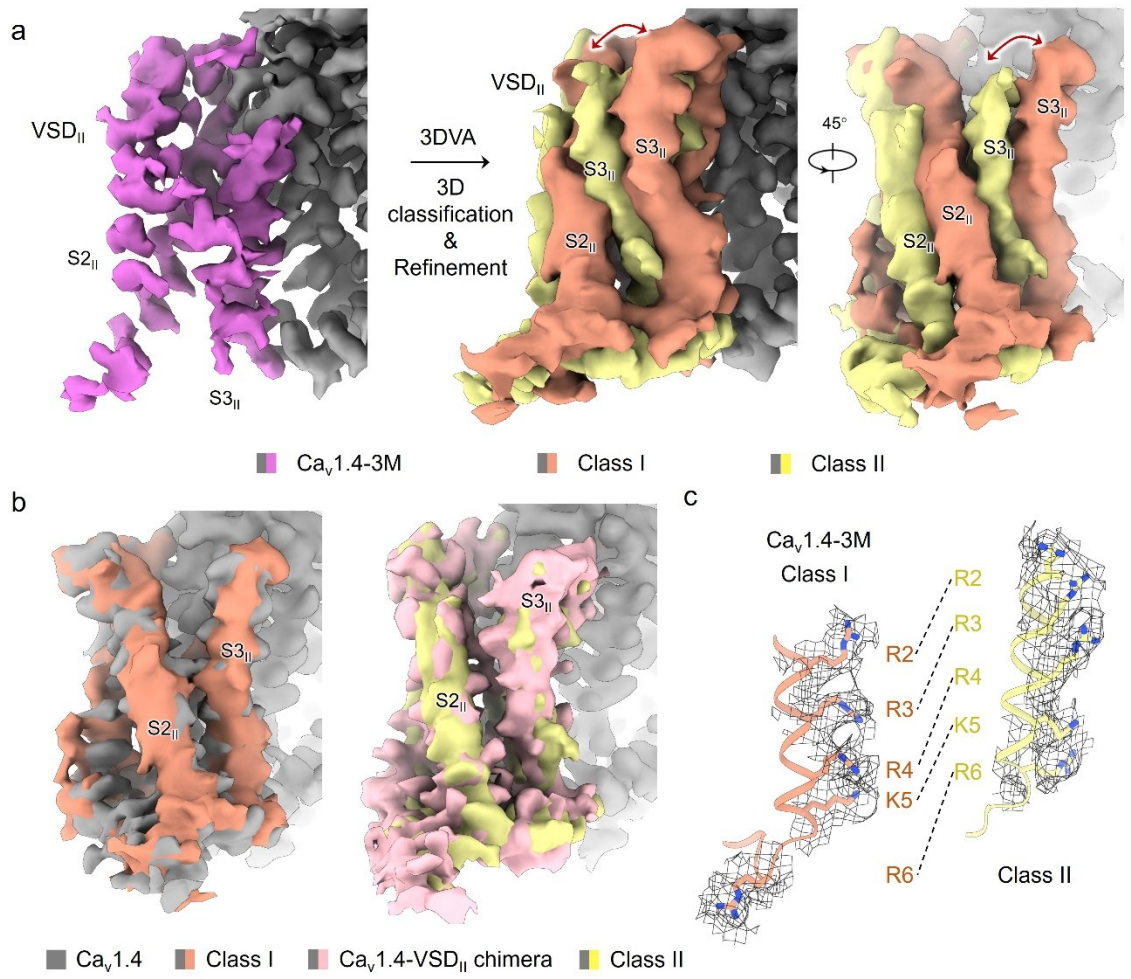

Figure S9 | Introducing triple mutations in Ca$_v$1.4 induces structural heterogeneity of VSD$_{II}$.

a, The poor local density for VSD$_{II}$ in Ca$_v$1.4-3M indicates increased structural dynamics of VSD$_{II}$ after the introduction of triple mutations. Subsequent 3DVA, 3D classification, and refinement of Ca$_v$1.4-3M generate two relatively stable conformations of VSD$_{II}$, termed Class I and Class II. The densities for VSD$_{II}$ in Ca$_v$1.4-3M, Class I, and Class II are shown in magenta, orange, and yellow, respectively. Red arrows indicate the structural shifts. **b,** Structural comparison reveals that the conformation of VSD$_{II}$ in Class I resembles that of WT Ca$_v$1.4, whereas that in Class II is similar to that of Ca$_v$1.4-VSD$_{II}$1.1 chimera. **c,** Local EM densities for S4$_{II}$ of Class I and Class II. S4$_{II}$ in Class I adopts a

"down" conformation, whereas that in Class II exhibits an "up" conformation. The EM density is contoured at 3.5 σ.

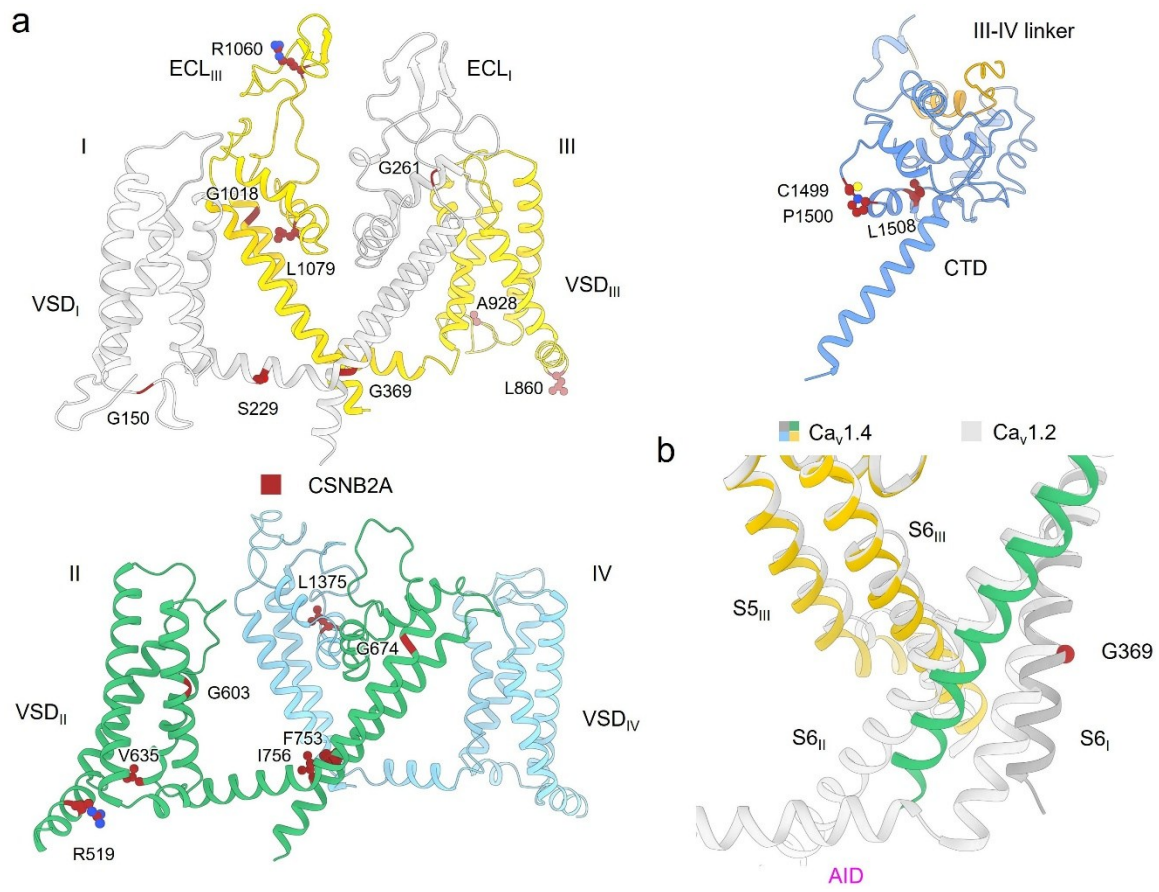

Figure S10 | Structural mapping of disease-associated mutations in Ca$_V$1.4.

a, Side views of repeat I and III, repeat II and IV, as well as the III-IV linker and CTD are shown. Please refer to Table S2 for details. CSNB2A: congenital stationary night blindness type 2A. **b,** G369, a disease-related mutation site, is located in S6$_I$ and marks the starting point of the conformational shift of S6$_I$.

Table S1 | Cryo-EM data collection, refinement and validation statistics.

	$Ca_v1.4$	$Ca_v1.1$	$Ca_v1.4$-$VSD_{II}1.1$	$Ca_v1.4$-3M Class I	$Ca_v1.4$-3M ClassII	$Ca_v1.4$-SR33805
Data collection and processing						
Magnification	64,000	64,000	64,000	64,000		64,000
Voltage (kV)	300	300	300	300		300
Electron exposure ($e^-/Å^2$)	50	50	50	50		50
Defocus range (μm)	-1.3 to -1.8	-1.3 to -1.8	-1.3 to -1.8	-1.3 to -1.8		-1.3 to -1.8
Pixel size (Å)	1.0979	1.0979	1.0979	1.0979		1.0979
Symmetry imposed	C1	C1	C1	C1		C1
Movies	6,763	6,065	3,095	4,060		6,231
Final particle images (No.)	173,010	161,461	203,971	103,265	114,198	281,113
Map resolution (Å)	2.89	2.90	3.30	2.93	2.87	2.87
FSC threshold	0.143	0.143	0.143	0.143	0.143	0.143
Refinement						
Map sharpening *B* factor ($Å^2$)	74.3	79.8	110.8	68.3	68.5	85.7
Model resolution (Å)	3.30	3.30	3.50	3.30	3.30	
FSC threshold	0.5	0.5	0.5	0.5	0.5	0.5
Model composition						
Non-hydrogen atoms	19,028	18,870	19,008	19,009	19,031	19,409
Protein residues	2,276	2,310	2,269	2,275	2,276	2,276
Ligands	38	23	38	38	38	39
B factors ($Å^2$)						
Protein	150.88	106.82	82.50	136.54	135.97	111.84
Ligand	157.29	123.79	101.42	136.64	142.85	104.86
R.m.s. deviations						
Bond lengths (Å)	0.004	0.005	0.004	0.003	0.003	0.003
Bond angles (°)	0.747	0.788	0.703	0.740	0.707	0.708
Validation						
MolProbity score	1.89	1.92	1.89	1.93	1.83	1.82
Clashscore	9.45	10.41	9.79	11.00	9.31	8.41
Poor rotamers (%)	0.65	0.49	0.30	0.25	0.60	0.30
Ramachandran plot						
Favored (%)	94.17	94.39	94.55	94.56	95.19	94.61
Allowed (%)	5.74	5.53	5.37	5.30	4.77	5.39
Outliers (%)	0.09	0.09	0.09	0.13	0.04	0.00

Table S2 | Disease-related mutations in $Ca_V1.4$.

Mutations	Disease	Location*	Mutations	Disease	Location
C74R	CSNB2A	NTD	I756T	CSNB2A	$I_{S6II,35}$
G150R	CSNB2A	$G_{S2I,39}$	L860P	CSNB2A	$L_{S1III,9}$
S229P	CSNB2A	$S_{S4I,50}$	A928D	CSNB2A	$A_{S2III,40}$
G261R	CSNB2A	$G_{S5I,45}$	G1018R	CSNB2A	$G_{S5III,34}$
G369D	CSNB2A	$G_{S6I,34}$	R1060W	CSNB2A	$R_{S5III,87}$
R519Q	CSNB2A	$R_{S1II,7}$	L1079P	CSNB2A	$L_{P2III,21}$
G603R	CSNB2A	$G_{S3II,36}$	L1375H	CSNB2A	$L_{P2IV,20}$
V635I	CSNB2A	$V_{S4II,37}$	C1499R	CSNB2A	CTD
G674D	CSNB2A	$G_{S5II,34}$	P1500R	CSNB2A	CTD
G753C	CSNB2A	$G_{S6II,32}$	L1508P	CSNB2A	CTD

CSNB2A: congenital stationary night blindness type 2

*The location information is based on the following reference:

Jin, X., Huang, J., Wang, H., Wang, K., & Yan, N. (2024). A versatile residue numbering scheme for Nav and Cav channels. *Cell Chemical Biology*, *31*(8), 1394-1404.

Disease mutations in structurally unresolved regions are shaded light grey. Mutations are summarized from https://www.uniprot.org/uniprotkb/O60840/entry#disease_variants.